Structural Engineering and Mechanics, Vol. 15, No. 2 (2003) 225-238
DOI: http://dx.doi.org/10.12989/sem.2003.15.2.225

Finite strip analysis of a box girder simulating the hull of a ship

G. Akhras† and J. P. Tremblay‡

Department of Civil Engineering, Royal Military College of Canada, Kingston, Ontario, Canada K7K 5L0

T. Graham‡†

Director Maritime Ship Support, Department of National Defence, Ottawa, Ontario, Canada K1A 0K2

M. S. Cheung‡‡ and W. C. Li‡‡†

Department of Civil & Environmental Engineering, Carleton University, 1125 Colonel By Drive, Ottawa Ontario, Canada K1S 5B6

(Received June 17, 2002, Accepted December 18, 2002)

Abstract. In the present study, the finite strip analysis of a box girder to simulate a ship's hull model is carried out to investigate its inelastic post-buckling behavior and to predict its ultimate flexural strength. Residual stresses and initial geometrical imperfections are both considered in the combined material and geometrical nonlinear analysis. The von-Mises yield criterion and the Prandtl-Reuss flow theory of plasticity are applied in modeling the elasto-plastic behavior of material. The Newton-Raphson iterative process is also employed in the analysis to achieve convergence. The numerical results agree well with the experimental data. The effects of some material and geometrical parameters on the ultimate strength of the structure are also investigated.

Key words: finite strip; inelastic post-buckling; ultimate strength; box girder; ship's hull.

1. Introduction

The hull of a ship is subjected concurrently to the hogging phenomenon which produces tension in the top deck and compression in the bottom while the sagging phenomenon will produce the opposite stress distribution. The loading patterns resulting from the hogging and sagging effects are

† Professor
‡ Research Assistant
‡† Project Manager
‡‡ Adjunct Professor
‡‡† Research Associate

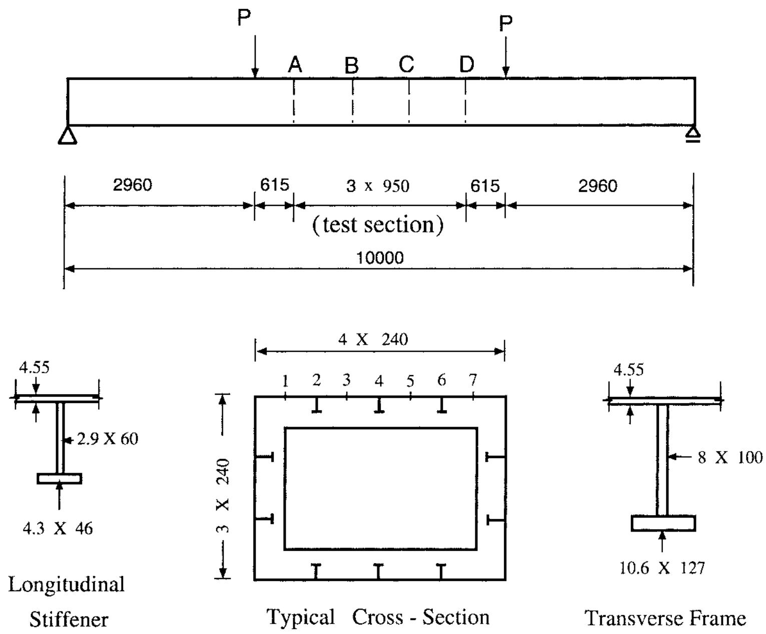

Fig. 1 RMC Model (All dimensions in millimetres)

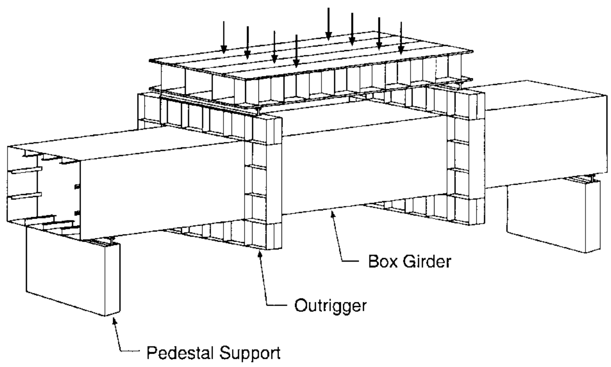

Fig. 2 A 3D view of the test model

very complex. Therefore, the ability to adequately describe the structural behavior of the hull, and the capability to accurately predict its ultimate strength are important topics in any ship structural design.

Many experimental research groups have carried out research on the ultimate strength of hulls. The models vary from a one third scale model of a typical hull to full-scale components of the ship. In recent years, the consensus reached is to test a box girder to simulate the behavior of the hull and predict its ultimate strength.

Recently, a box girder (Figs. 1 and 2) was built and tested at the Royal Military College of Canada (Akhras 1996). This model was fabricated following typical hull construction methods, and was loaded with pure bending until failure occurred. In this experiment, the structural behavior was studied and the results were compared with predictions of a current design method (Akhras *et al.* 1998).

As a part of this effort, a finite strip analysis of the box girder is carried out in order to simulate numerically the inelastic post-buckling behavior of the model and to investigate the effects of some parameters on the ultimate strength of the structure. The finite strip method uses a series of trigonometric functions or B-spline functions to describe the longitudinal profile of the displacement components (Cheung *et al.* 1996). Therefore, the dimensions of the analysis are reduced and a significant computational saving is achieved. This method has been successfully employed to investigate the post-buckling behaviors of many plate structures and has shown its satisfactory performance (e.g., Hancock 1981, Sridharan & Graves-Smith 1981, Guo & Lindner 1993, Wang & Dawe 1996, Dawe & Wang 1998, and Dawe 2002)

In this analysis, only one longitudinal segment (AB of Fig. 1) confined between two adjacent transverse frames is included. These frames are very strong so that the end cross-sections of the segment can be assumed to remain plane during the deformation under pure bending. This deformation pattern is modeled by means of a carefully selected shape function for longitudinal displacement. In addition, residual stresses and initial geometrical imperfections are both considered in the combined geometrically and materially nonlinear simulation. The von-Mises yield criterion and the Prandtl-Reuss flow theory of plasticity are employed in modeling the elasto-plastic behavior of the material and the Newton-Raphson iteration is performed as the rotation of the end cross-sections of the structure is increased step by step. The parameter representing the overall axial strain of the structure is adjusted constantly during the solution process in order to eliminate the resulting overall axial force on any cross-section of the structure in compliance with the assumption of zero axial force in pure bending.

The numerical results agree reasonably well with the experimental data. The effects of some material and geometrical parameters on the ultimate strength of the structure are also investigated.

2. Displacement functions

In finite strip analysis, a thin-walled structure is modeled by a number of longitudinal flat shell strips (Cheung *et al.* 1996), each of which has three equally spaced nodal lines (Figs. 3 and 4). In the transverse direction of the strip, the quadratic interpolation is used for in-plane deformation whilst the Hermitian cubic polynomials are employed for out-of-plane bending. The strip is hinged

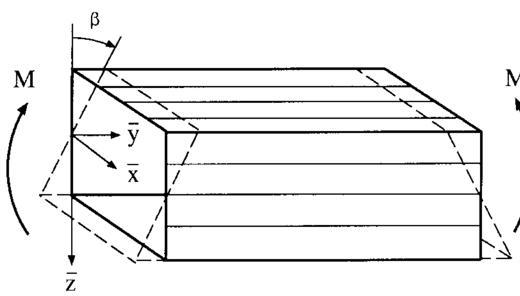

Fig. 3 Box girder under pure bending

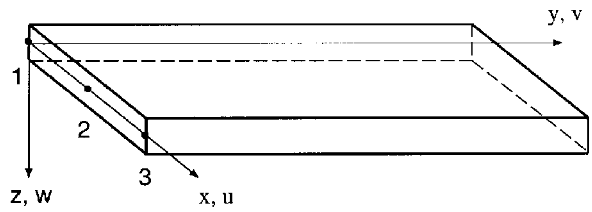

Fig. 4 A finite strip

at both ends and the end cross-sections are assumed to remain plane during deformation. Moreover, the displacements of two adjacent strips along any corner line of the structure must be compatible. These conditions can be satisfied by the following displacement functions:

$$u = \sum_{m=1}^{r} \sum_{i=1}^{3} N_i(x) u_{im} \sin\frac{m\pi y}{l}$$

$$v = \sum_{m=1}^{r} \sum_{i=1}^{3} N_i(x) v_{im} \sin\frac{(m+1)\pi y}{l} + \beta \bar{z}\left(\frac{2y}{l} - 1\right) + \alpha y$$

$$w = \sum_{m=1}^{r} \sum_{i=1,3} \left[F_i(x) w_{im} + H_i(x)\left(\frac{\partial w}{\partial x}\right)_{im}\right] \sin\frac{m\pi y}{l} \quad (1)$$

where

u and v are the in-plane displacements of the point (x, y, 0) on the midplane;

w is the deflection which is assumed to be constant in the thickness direction z;

r is the number of harmonics employed in the analysis;

u_{im}, v_{im}, w_{im} and $\left(\frac{\partial w}{\partial x}\right)_{im}$ are the displacement parameters for the i-th nodal line and the m-th harmonic;

l is the length of the strip;

$N_i(x)$ is the quadratic interpolation function for nodal line i (i = 1 to 3) with the following expression:

$$N_i(x) = \prod_{\substack{j=1 \\ j \neq i}}^{3} \frac{x - x_j}{x_i - x_j} \quad (2)$$

$F_i(x)$ and $H_i(x)$ (i = 1, 3) are the Hermitian cubic polynomials as below:

$$F_1(x) = 1 - 3X^2 + 2X^3$$

$$F_3(x) = 3X^2 - 2X^3$$

$$H_1(x) = x[1 - 2X + X^2]$$

$$H_3(x) = x[X^2 - X] \quad (3)$$

with b denoting the width of the strip, while $X = x/b$;

β is the rotation of each end cross-section (Fig. 3), its value is given as external load;

$\bar{z}$ is the global vertical coordinate with the origin located on the elastic neutral axis of structural cross-section (Fig. 3);

α is the longitudinal strain due to global elongation of the structure at level $\bar{z} = 0$. Its value is assumed to be zero initially and is adjusted constantly during iteration to eliminate the axial force of the structure as mentioned later.

3. Strains and stresses

Including the effects of initial geometrical imperfections u_0 and w_0, the following strain-displacement relationships are used:

$$\varepsilon_x = \bar{\varepsilon}_x - z\frac{\partial^2(w-w_0)}{\partial x^2}$$

$$\varepsilon_y = \bar{\varepsilon}_y - z\frac{\partial^2(w-w_0)}{\partial y^2}$$

$$\gamma_{xy} = \bar{\gamma}_{xy} - 2z\frac{\partial^2(w-w_0)}{\partial x \partial y} \tag{4}$$

where $\bar{\varepsilon}_x$, $\bar{\varepsilon}_y$, and $\bar{\gamma}_{xy}$ are the strains of the midplane and are defined as

$$\bar{\varepsilon}_x = \frac{\partial(u-u_0)}{\partial x} + \frac{1}{2}\left[\left(\frac{\partial w}{\partial x}\right)^2 - \left(\frac{\partial w_0}{\partial x}\right)^2\right]$$

$$\bar{\varepsilon}_y = \frac{\partial v}{\partial y} + \frac{1}{2}\left[\left(\frac{\partial w}{\partial y}\right)^2 - \left(\frac{\partial w_0}{\partial y}\right)^2\right] + \underline{\frac{1}{2}\left[\left(\frac{\partial u}{\partial y}\right)^2 - \left(\frac{\partial u_0}{\partial y}\right)^2\right]}$$

$$\bar{\gamma}_{xy} = \frac{\partial(u-u_0)}{\partial y} + \frac{\partial v}{\partial x} + \left[\frac{\partial w}{\partial x}\frac{\partial w}{\partial y} - \frac{\partial w_0}{\partial x}\frac{\partial w_0}{\partial y}\right] \tag{5}$$

The underlined term in the expression of $\bar{\varepsilon}_y$ accounts for the nonlinear effect of membrane displacement. The other nonlinear terms are considered to be of secondary importance and have been neglected in the above equations.

In the elastic stage, the linear stress-strain relationships hold:

$$\begin{Bmatrix} \sigma_x \\ \sigma_y \\ \tau_{xy} \end{Bmatrix} = \frac{E}{1-\nu^2}\begin{bmatrix} 1 & \nu & \\ \nu & 1 & \\ & & \frac{1-\nu}{2} \end{bmatrix}\begin{Bmatrix} \varepsilon_x \\ \varepsilon_y \\ \gamma_{xy} \end{Bmatrix} + \begin{Bmatrix} \sigma_{x0} \\ \sigma_{y0} \\ \tau_{xy0} \end{Bmatrix} \tag{6}$$

or in a compact form

$$\{\sigma\} = [\sigma_x, \sigma_y, \tau_{xy}]^T = [D]\{\varepsilon\} + \{\sigma_0\} \tag{7}$$

where $[D]$ is the elastic matrix of the material and $\{\sigma_0\} = [\sigma_{x0}, \sigma_{y0}, \tau_{xy0}]^T$ represents the initial residual stresses generated during the fabrication process.

According to the von-Mises criterion, the material yields when the equivalent stress $\bar{\sigma}$ reaches the uniaxial yield stress σ_Y:

$$\bar{\sigma} = \sqrt{\sigma_x^2 + \sigma_y^2 - \sigma_x\sigma_y + 3\tau_{xy}^2} = \sigma_Y \tag{8}$$

After yielding, the stresses can be calculated using the incremental stress-strain relationship:

$$d\{\sigma\} = [D]_{ep}d\{\varepsilon\} = [D]d\{\varepsilon\} - [D]_p d\{\varepsilon\} \tag{9}$$

where $[D]_{ep} = [D] - [D]_p$ is the elasto-plastic matrix and $[D]_p$ is the plastic matrix which can be formed from the current stress level according to the Prandtl-Reuss flow theory of plasticity. The related theoretical foundation of this procedure is well known. Because it is described in details elsewhere (Zienkiewicz 1977, Owen *et al.* 1980), it will not be repeated here. In the present analysis, the following steps are used for elastic-perfectly plastic material after yielding:

First, only the elastic part of the stress increments $[D]d\{\varepsilon\}$ is added to the stresses obtained in the previous loading step:

$$\{\sigma\}_e = \{\sigma\}^k + [D]\{\{\varepsilon\} - \{\varepsilon\}^k\} \tag{10}$$

where $\{\varepsilon\}$ is the current value of the strain vector; $\{\sigma\}^k$ and $\{\varepsilon\}^k$ are respectively the last values of the stress and strain vectors in the previous loading step k.

Then, the equivalent stress $\bar{\sigma}_e$ of $\{\sigma\}_e$ is calculated using Eq. (8). If $\bar{\sigma}_e$ is smaller than σ_Y, unloading occurs in the region under consideration, and the elastic relationship is used. Therefore, the current stress vector is

$$\{\sigma\} = \{\sigma\}_e \tag{11}$$

Otherwise with $\bar{\sigma}_e$ greater than or equal to σ_Y, the plastic deformation occurs and Eq. (9) stands. Thus, the second part of the stress increments in Eq. (9) must be included:

$$\{\sigma\} = \{\sigma\}_e - [D]_p(\{\varepsilon\} - \{\varepsilon\}^k) \tag{12}$$

where

$$[D]_p = \frac{E}{Q(1-\nu)^2}\begin{bmatrix} (S_1+\nu S_2)^2 & & \mathit{Symm.} \\ (S_1+\nu S_2)(S_2+\nu S_1) & (S_2+\nu S_1)^2 & \\ (S_1+\nu S_2)S_3 & (S_2+\nu S_1)S_3 & S_3^2 \end{bmatrix} \tag{13}$$

in which

$$S_1 = \sigma_x^k - (\sigma_x^k + \sigma_y^k)/3$$

$$S_2 = \sigma_y^k - (\sigma_x^k + \sigma_y^k)/3$$

$$S_3 = (1-\nu)\tau_{xy}^k$$

$$Q = S_1^2 + S_2^2 + 2\nu S_1 S_2 + 2S_3^2/(1-\nu)$$

and the superscript k represents the previous loading step.

Thereafter, the stresses obtained from Eq. (12) is brought to yield surface using

$$\{\sigma\}_{new} = \frac{\sigma_Y}{\bar{\sigma}}\{\sigma\} \tag{14}$$

where $\bar{\sigma}$ is the equivalent stress of $\{\sigma\}$.

4. Solution procedure

The entire loading process is carried out in a number of steps. In each step, the end rotation β of the structure is increased by a small increment, and the Newton-Raphson iterations are implemented until convergence occurs.

Each finite strip is divided into several layers through out the thickness. In each iteration, after the strains and stresses are computed at the level of each layer, the tangential stiffness matrix and the vector of unbalanced loads (Cheung *et al*. 1996) are updated. The value of α is assumed to be zero initially with the origin of $\bar{z}$ located on the elastic neutral axis. Afterwards, its value is modified according to the resulting average axial force and average axial stiffness of the structure in each iteration:

$$\alpha^{n+1} = \alpha^n - \frac{\iiint\limits_V \sigma_y dxdydz}{\iiint\limits_V D_{ep22} dxdydz} \tag{15}$$

where

V denotes the volume of entire structure;

n is the sequential number of iteration;

D_{ep22} is the second diagonal item of $[D]_{ep}$ and is defined as

$$D_{ep22} = \begin{cases} \dfrac{E}{1-\nu^2} & \text{for elastic region} \\ \dfrac{E}{1-\nu^2} - D_{p22} & \text{for plastic region} \end{cases} \tag{16}$$

where D_{p22} is the item of $[D]_p$ given in Eq. (13).

Thus, the axial force at any cross-section of the structure is reduced to a minimum in compliance with the assumption of zero axial force in pure bending.

Based on the updated value of α, the stress σ_y can be recalculated. Then, the average value of the bending moment on any cross-section of the girder is obtained as

$$M = \frac{1}{l}\iiint\limits_V \sigma_y \bar{z}\, dxdydz \tag{17}$$

in which l is the length of the structure, M is the average value of the bending moment over the length of the structure and $\bar{z}$ is the structural vertical coordinate. The location of the origin of $\bar{z}$ has negligible influence on the value of M since the axial force is zero.

5. Numerical results

5.1 The RMC model

As shown in Figs. 1 and 2, the model simulating the hull and tested at the Royal Military College of Canada is a 10 meter long box-girder, which is simply supported at both ends and loaded symmetrically with two point forces. Under such configuration, the middle portion is subjected to a uniform bending. This middle portion is divided into three segments by four heavy transverse frames. The two outer sections and outriggers were designed to transfer the loads without any significant deformation. The measured average values of the steel properties are E = 205.34 GPa and σ_Y = 317.85 MPa for the longitudinal stiffeners; E = 211.62 GPa and σ_Y = 293.72 MPa for the plating. Further, ν = 0.3 is assumed for both the plating and the stiffeners.

The transverse frames are introduced to provide a proper support for the longitudinal stiffeners and their attached plating. They are strong enough not to fail before the failure of the longitudinal stiffened panels. This implies that the buckling of the inter-frame panels will occur before the overall collapse of the box girder. Consequently, it is reasonable to assume first that the box cross section at the location of the transverse frames will remain plane during the local buckling process and second that modeling only one segment confined between two adjacent transverse frame is sufficient to represent the general behavior of the test section.

As mentioned previously, in parallel with the experimental study, a finite strip method is proposed in this work to simulate the post-buckling behavior of the box girder. The model consists of eighty five (85) finite strips of 6 layers combined with (11) series terms (Fig. 5). It was found that a further refined model could only yield little improvement to the analysis. The initial geometrical

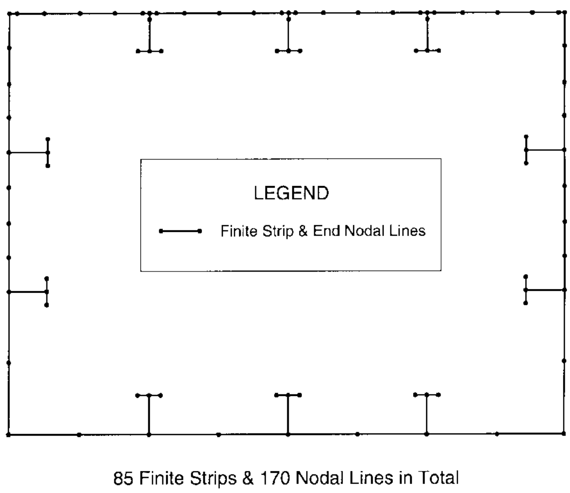

Fig. 5 Finite strip model of box girder

imperfections and residual stresses are included in the analysis in the following fashion.

In each segment, the initial deflection w_0 of the model were measured at three points along each longitudinal stiffener and the center line of each plate panel before loading was applied. These lines are chosen as the nodal lines of the finite strip model (Fig. 5). From Eq. (1), the measured initial deflection w_0 at point k with the longitudinal coordinate $y = y_k$ on any nodal line is equal to

$$w_0^k = \sum_{m=1}^{3} w_{0m} \sin\frac{m\pi y_k}{l}$$

which yields three equations for k = 1, 2, 3 that can easily be solved for w_{0m} from the measured values of w_0^k. The results for w_{0m} along line 1 to 7 on the top plate (Fig. 1) are summarized in Table 1, in which the positive direction of w is downwards. Furthermore, the initial deflections and slopes of the top plate along any nodal lines for any series terms are evaluated by means of spline function interpolations (Cheung *et al*. 1996).

To model the residual stresses, the recommendation of Skaloud and Zornerova (1984) are followed. The residual stresses σ_{y0} are assumed equal to the yield stress σ_Y of the material within a width of 3 times the thickness beside each weld, and its negative values in the adjacent areas should counterbalance this positive stress, i.e., $\sigma_{y0} = -6t^2\sigma_Y/t(b_p - 6t) = -37.7$ MPa in each top panel and $\sigma_{y0} = -3t^2\sigma_Y/(A_l - 3t^2) = -22.3$ MPa in the top stiffeners, where t is the thickness of the top plate or stiffener web, b_p represent the width of each top panel and A_l denotes the area of each longitudinal stiffener. The initial deflection and the residual stress in the components other than the top plate and top stiffeners are neglected because of their insignificant influence on the structural behavior.

First, the linear stability analysis of this model is completed. The resulting lowest critical moment is M_{cr} = 1476 kN-m at the end rotation $\beta_{cr} = 0.2003 \times 10^{-2}$ radian and m = 4, whilst the second critical moment is M_{cr} = 1486 kN-m at $\beta_{cr} = 0.2016 \times 10^{-2}$ radian and m = 5. Apparently, these two critical moments are close to each other and slightly lower than the ultimate plastic moment M_p = 1558 kN-m obtained using the beam theory. Moreover, the two buckling modes are both anti-symmetrical to the center of top plate.

Then, the inelastic post-buckling finite strip simulation is carried out. The results of bending moment M and maximum displacement parameters w_m for series terms m = 1 to m = 5 versus the end rotation β are listed in Table 2. The volume of yield zone is also given in this table as a

Table 1 Initial geometrical imperfections of RMC model

Longitudinal line in Fig. 1	W_{0m} (mm)		
	m = 1	m = 2	m = 3
1	3.45	–0.34	0.58
2	3.13	–0.54	0.56
3	3.65	–0.00	0.67
4	1.47	–0.10	0.41
5	2.89	0.25	0.40
6	2.33	0.71	0.21
7	4.22	0.67	0.51

Table 2 Finite strip simulation of the RMC model under pure bending

β (10^{-2})	Maximum w_m (mm)					M (kN-m)	Volume of yield (%)
	m = 1	m = 2	m = 3	m = 4	m = 5		
0.05	4.578	0.849	0.855	0.005	0.010	373	0
0.10	4.905	0.919	1.064	0.014	0.032	746	0
0.15	5.257	0.997	1.445	0.090	0.132	1117	1.2
0.16	5.327	1.095	1.523	0.757	0.349	1165	7.5
0.17	5.245	1.298	1.637	1.255	0.345	1191	9.8
0.18	5.219	1.441	1.809	1.541	0.339	1221	11.8
0.19	5.227	1.570	1.961	1.780	0.338	1248	14.3
0.20	5.271	1.694	2.093	2.000	0.351	1262	19.4
0.21	5.460	1.810	2.198	2.197	0.363	1273	28.1
0.22	5.706	1.925	2.268	2.387	0.367	1274	31.0
0.23	5.950	2.030	2.304	2.570	0.372	1273	31.7
0.24	6.190	2.115	2.298	2.745	0.377	1271	33.4
0.25	6.437	2.173	2.257	2.913	0.382	1270	34.0
0.26	6.687	2.205	2.194	3.074	0.386	1268	36.2

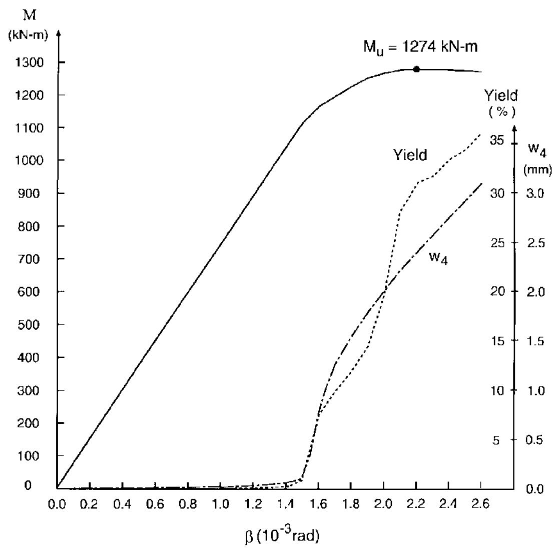

Fig. 6 Results of finite strip analysis of RMC model

percentage of the entire volume of the box.

It can be seen from the results that as the end rotation β increases and approaches to its critical value, the critical mode m = 4 grows drastically and the plastic deformation spreads massively. These two effects reduce the stiffness of the box significantly and eventually lead to structural failure after the bending moment reaches its maximum value M_u =1274 kN-m at $\beta = 0.220 \times 10^{-2}$, as shown in Fig. 6. The experimental result of M_u is 1238 kN-m, which is in a close agreement with the finite strip result.

5.2 Effects of initial geometrical imperfections

In order to investigate the effects of the initial geometrical imperfections, the finite strip analysis is repeated for the RMC model with different levels of initial geometrical imperfections $k\{w_0\}$, where $\{w_0\}$ is the measured value of the initial geometrical imperfections of the present model, and with other parameters unchanged. For k = 0.1, 1.0, 1.5 and 2.0, the results are given in Table 3.

It can be seen that the lower geometrical imperfections yield higher bending moment at the beginning of the loading process. However, as the end rotation keeps increasing, the compression stresses in the top plate build up more quickly in the structure with lower initial geometrical imperfections. For k = 0.1 (very low initial geometrical imperfections), the top plate buckles and the buckling mode ($m = 5$) becomes dominant in the overall deformation pattern after $\beta \geq 0.1525 \times 10^{-2}$, which leads to a reduced ultimate strength (1269 kN-m). In contrast, in the structures with higher initial geometrical imperfections, the deformation mode m = 1 remains dominant in the deflection pattern during the entire loading process, which yields favorable effects on maintaining a relatively uniform distribution of the compression stress in the top plate and eventually leads to a higher ultimate strength (1295 kN-m for k = 2.0). However, for the present model, the ultimate strength is not very sensitive to the amount of initial geometrical imperfections. The twenty times of variation in the initial geometrical imperfections corresponding to the change of k from 0.1 to 2.0 only results in two percent difference in the ultimate strength of the model.

5.3 Effects of the initial residual stresses

To evaluate the impact of the initial residual stresses on the ultimate moment, a series of simulation on the RMC model is undertaken. The residual stress level is reduced to half and zero

Table 3 Effects of initial geometrical imperfections

β (10^{-2})	M (kN-m)			
	k = 0.1	k = 1.0	k = 1.5	k = 2.0
0.05	375	373	370	368
0.10	752	746	741	736
0.15	1128	1117	1109	1101
0.16	1132	1165	1172	1165
0.17	1167	1191	1200	1213
0.18	1200	1221	1225	1239
0.19	1227	1248	1249	1263
0.20	1245	1262	1268	1280
0.21	1256	1273	1277	1288
0.22	1262	1274	1281	1294
0.23	1266	1273	1281	1295
0.24	1269	1271	1279	1295
0.25	1268	1270	1279	1293
0.26	1267	1268	-	1292
M_u	1269	1274	1281	1295

Table 4 Effects of residual stresses

β (10^{-2})	M (kN-m) At residual stresses level:		
	Zero	half	full
0.05	374	374	373
0.10	748	747	746
0.15	1121	1119	1117
0.16	1194	1193	1165
0.17	1266	1246	1191
0.18	1321	1268	1221
0.19	1300	1286	1286
0.20	1300	1290	1262
0.21	1295	1288	1273
0.22	-	1283	1274
0.23	-	-	1273
M_u	1321	1290	1274

Table 5 Effects of yield stress σ_Y

β (10^{-2})	M (kN-m)		
	σ_Y = 400 MPa	RMC model	σ_Y = 250 MPa
0.05	372	373	373
0.10	746	746	747
0.15	1117	1117	1046
0.16	1190	1165	1066
0.17	1259	1191	1077
0.18	1314	1221	1080
0.19	1348	1248	1081
0.20	1385	1262	1081
0.21	1424	1273	1078
0.22	1458	1274	1075
0.23	1482	1273	-
0.24	1503	1271	-
0.28	1560	-	-
0.32	1602	-	-
0.36	1611	-	-
0.40	1607	-	-
M_u	1611	1274	1081
M_u/M_{cr}	1.091	0.863	0.732
M_u/M_p	0.770	0.818	0.827

respectively and all other parameters are unchanged. The results indicate that M_u rises by 3.7 percent if there is no residual stresses due to fabrication (Table 4).

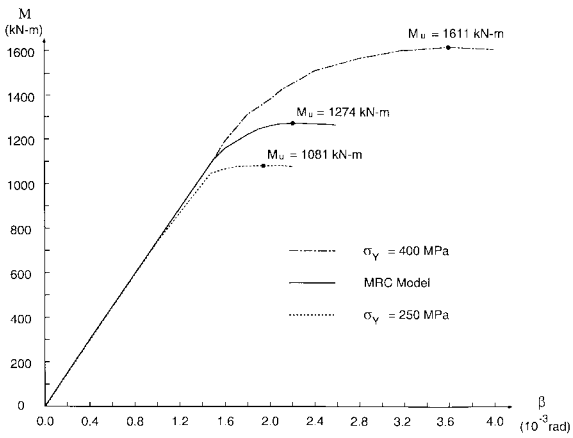

Fig. 7 Effects of yield stress

5.4 Effects of yield stress σ_Y

The RMC model is further analyzed for different values of yield stress σ_Y. Accordingly, the level of residual stress is also modified in proportion to σ_Y with all other parameters remaining unchanged. The results of the present model with the ones for σ_Y = 400 MPa (M_p = 2091 kN-m) and 250 MPa (M_p = 1307 kN-m) are summarized in Table 5 and illustrated in Fig. 7. It can be concluded that a higher σ_Y yields a higher M_u/M_{cr} but a lower M_u/M_p.

6. Conclusions

In the present study, the finite strip analysis is carried out to investigate the post-buckling behavior of a box girder under pure bending simulating the hull of a ship. The resulting ultimate moment is M_u = 1274 kN-m, which agrees well with the experimental result M_u = 1238 kN-m. The minor discrepancy between numerical and experimental results is mainly attributed to simplifications in modeling the initial geometrical imperfections, initial residual stresses, deformation pattern of end cross-sections, as well as the elasto-plastic behavior of materials.

Numerical results indicate that the ultimate moment M_u of the present model is not sensitive to the magnitude of the initial geometrical imperfections; its ultimate moment can be increased by 3.7 percent if there is no residual stress due to fabrication; and using the materials with higher yield stress results in a higher ratio of the ultimate moment over the critical one M_u/M_{cr} but a lower ratio of the ultimate moment over the plastic one M_u/M_p.

Acknowledgements

The financial supports from the Department of National Defence and the Natural Sciences and Engineering Research Council of Canada are gratefully acknowledged.

References

Akhras, G. (1996), "Determining the ultimate strength of ship's hull", Final Report and Appendices, Royal Military College of Canada.

Akhras, G., Gibson, S., Yang, S. and Morchat, R. (1998), "Ultimate strength of a box girder simulating the hull of a ship", *Canadian Journal of Civil Engineering*, **25**(5), 829-843.

Cheung, M.S., Li, W. and Chidiac, S.E. (1996), *Finite Strip Analysis of Bridges*, E & FN SPON, London.

Dawe, D.J. (2002), "Use of finite strip method in predicting the behaviours of composite laminated structures", *Composite Structures*, **57**(1), 11-36.

Dawe, D.J. and Wang, S. (1998), "Postbuckling analysis of thin rectangular laminated plates by spline FSM", *Thin-Walled Structures*, **30**(1-4), 159-179.

Guo, Y.L. and Lindner, J. (1993), "Analysis of elasto-plastic interaction buckling of stiffened panels by spline finie strip method", *Computers & Structures*, **46**(3), 529-536.

Hancock, G.J. (1981), "Nonlinear analysis of thin sections in compression", *J. Struct. Div., Proc.*, ASCE, **107**(ST3), 455-471.

Owen, D.R.J. and Hinton, E. (1980), *Finite Element in Plasticity (Theory and Practice)*, Pineridge Press, Swansea.

Skaloud, M. and Zornerova, M. (1984), "Effect of residual stresses on the stability problem of longitudinally stiffened compression flanges", *Acta Technical*, CSAV **20**, 253.

Sridharan, S. and Graves-Smith, T.R. (1981), "Postbuckling analyses with finite strips", *J. Eng. Mech. Div., Proc*. ASCE, **107**(EM5), 869-888.

Wang, S. and Dawe, D.J. (1996), "Finite strip large deflection and post-overall-buckling analysis of diaphragm-supported plate structures", *Computers & Structures*, **61**(1), 155-170.

Zienkiewicz, O.C. (1977), *The Finite Element Method*, third edt., McGRAW-HILL, UK.